Interferon-alpha enhances the antitumour activity of EGFR-targeted therapies by upregulating RIG-I in head and neck squamous cell carcinoma

Hailong Ma[1,4], Shufang Jin[1,4], Wenyi Yang[1], Ge Zhou[2], Mei Zhao[2], Sijie Fang[3], Zhiyuan Zhang*,[1] and Jingzhou Hu*,[1]

[1]Department of Oral Maxillofacial-Head and Neck Oncology, Shanghai Ninth People's Hospital, Shanghai Jiao Tong University School of Medicine, Shanghai Key Laboratory of Stomatology, Shanghai 200011, China; [2]Department of Head and Neck Surgery, The University of Texas MD Anderson Cancer Center, Houston, TX 77030, USA and [3]Department of Ophthalmology, Shanghai Ninth People's Hospital, Shanghai Jiao Tong University School of Medicine, Shanghai 200011, China

Background: The epidermal growth factor receptor (EGFR)-targeted therapies have been tested in the clinic as treatments for head and neck squamous cell carcinoma (HNSCC). Owing to intrinsic or acquired resistance, EGFR-targeted therapies often lead to a low response rate and treatment failure. Interferon-alpha (IFNα) is a chemosensitising agent and multi-functional cytokine with a tumour inhibitory effect. However, the synergic effect of IFNα and EGFR-targeted therapies (erlotinib and nimotuzumab) and their mechanisms in HNSCC remain unclear.

Methods: The interactions between IFNα, erlotinib, and nimotuzumab were evaluated in vitro in HNSCC cells. The synergistic effect of IFNα (20 000 IU per day, s.c.), erlotinib (50 mg kg^{-1} per day, i.g.) and nimotuzumab (10 mg kg^{-1} per day, i.p.) was further confirmed in vivo using HNSCC xenografts in nude mice. The upregulation of retinoic-acid inducible gene I (RIG-I) induced by IFNα and EGFR-targeted therapies and its mechanism were detected in vitro and in vivo.

Results: IFNα enhances the antitumour effects of erlotinib and nimotuzumab on HNSCC cells both in vitro and in vivo. Importantly, both IFNα and EGFR-targeted therapies promote the expression of RIG-I by activating signal transducers and activators of transcription 1 (STAT1) in HNSCC cells. RIG-I knockdown reduced the sensitivity of HN4 and HN30 cells to IFNα, erlotinib, and nimotuzumab. Moreover, IFNα transcriptionally induced RIG-I expression in HNSCC cells through STAT1.

Conclusions: IFNα enhances the effect of EGFR-targeted therapies by upregulating RIG-I, and its expression may represent a predictor of the effectiveness of a combination treatment including IFNα in HNSCC.

Epidermal growth factor receptor (EGFR) is overexpressed and structurally altered in head and neck squamous cell carcinomas (HNSCC) and is believed to have an important role in promoting the malignant progression of tumours, providing a strong rationale for the development and implementation of EGFR-targeted therapies for HNSCC (Sharafinski et al., 2010; Braig et al., 2017). Most EGFR inhibitors are classified into one of two categories: monoclonal antibodies (mAbs) (e.g., cetuximab, nimotuzumab,

and panitumumab) that bind the extracellular domain of EGFR and tyrosine kinase inhibitors (TKIs) (e.g., erlotinib and gefitinib) that competitively bind the intracellular ATP-binding pocket of EGFR, disrupting the kinase function (Imai and Takaoka (2006); Agulnik, 2012). However, EGFR inhibitors, including mAbs and TKIs, have only achieved modest success in treating recurrent and/ or metastatic HNSCC (Sacco, Cohen (2015)). The addition of panitumumab to chemotherapy did not improve overall survival in an unselected population of patients with recurrent or metastatic HNSCC (Vermorken et al., 2013). Multiple therapies targeting EGFR have been tested in patients with HNSCC, but the low response rates and intrinsic or acquired resistance usually lead to treatment failure (Vermorken et al., 2008; Martinez-Useros and Garcia-Foncillas (2015); Wen, Grandis (2015)). Studies aiming to identify methods to enhance the antitumour activity of EGFR inhibitors as treatments for HNSCC are particularly important and urgent.

Interferon-alpha (IFNα) has been approved as a treatment for several tumours, such as malignant melanoma, hairy leukaemia, non-Hodgkin lymphoma, Kaposi's sarcoma, and renal cell carcinoma (Parker et al., 2016). However, it is not approved for most solid tumours. IFNα produced by tumour cells and immune cells activates anticancer immunity by promoting the activity of T cells, natural killer (NK) cells, and dendritic cells (DC), as well as inhibiting the activity of immunosuppressive cells (Joffre et al., 2012; Bacher et al., 2013; Srivastava et al., 2014; Parker et al., 2016). IFNα has been shown to enhance the erlotinib-induced inhibition of proliferation in human bladder cancer and colon cancer (Yang et al., 2005; 2007) and to increase the sensitivity of human lung cancer to nimotuzumab (Diaz et al., 2009). IFNα induces apoptosis and potentiates EGFR expression in human epidermoid carcinoma KB cells (Caraglia et al., 1999). The synergistic antitumour activity of gefitinib (a TKI of EGFR) and IFNα has been observed in HNSCC (Bruzzese et al., 2006). Obviously, nimotuzumab and erlotinib utilise different mechanisms to block EGFR activation. Researchers have not yet clearly determined whether the combination of IFNα and EGFR-targeted therapies, including both nimotuzumab and erlotinib, exerts a synergistic effect on HNSCC. The retinoic-acid inducible gene I (RIG-I)-like receptors (RLRs) are a family of cytosolic pattern recognition receptors that are essential for detecting viral RNA and initiating the innate immune response (Weber-Gerlach, Weber (2016)). RIG-I is one of the most important RLPs. As shown in our previous study, high levels of activated RIG-I induce apoptosis and IFNα production in HNSCC (Hu et al., 2013). Therefore, we speculated that RIG-I may be involved in the mechanism underlying the effects of a combination treatment of IFNα and EGFR-targeted therapies. Further investigations are required to determine whether RIG-I is involved in the mechanism of the IFNα combination treatment and predicts the sensitivity of HNSCC to IFNα and EGFR-targeted therapies.

In the present study, we examined the synergistic effects of IFNα, erlotinib, and nimotuzumab on HNSCC in vivo and in vitro. The upregulation of RIG-I was described as a novel mechanism for the effects of the IFNα combination treatment on HNSCC. Moreover, RIG-I expression may help guide the clinical application of the IFNα combination treatment of HNSCC in the future.

MATERIALS AND METHODS

Cell culture. The cell lines used in this study were HN4 and HN30. HN4 cells originated from human tongue squamous carcinoma, whereas HN30 cells originated from human pharyngeal squamous cell carcinoma. Both the HN lines were kindly provided by Professor Mao Li, Department of Oncology and Diagnostic Sciences, University of Maryland School of Dentistry, University of Maryland and verified by STR genotyping. Cal27, a tongue squamous cell carcinoma cell line, was purchased from ATCC (Manassas, VA, USA). The EGFR inhibitors-resistant cell lines were constructed by gradually selection with targeted drugs using Cal27 cell line. In brief, the cells were first exposed to $0.5\,\mu M$ erlotinib or $50\,\mu g\,ml^{-1}$ nimotuzumab for 72 h. The surviving cells were then split and exposed to higher doses of drugs for 2–3 days per week for ~4 weeks. The resistant cells were named Cal27/ erlotinib and Cal27/nimotuzumab, and maintained in normal culture medium containing $5\,\mu M$ erlotinib or $200\,\mu g\,ml^{-1}$ nimotuzumab. The cell lines were cultured in Dulbecco's Modified Eagle's Medium (Gibco, Grand Island, NY, USA) supplemented with 10% foetal bovine serum, 1% glutamine, and 1% penicillin– streptomycin. Cells were cultured in a humidified atmosphere of 5% CO_2 at 37 °C.

Transfection. Cells were transiently transfected with siRNAs or plasmids using Lipofectamine 3000 (Invitrogen, Carlsbad, CA, USA), according to the manufacturer's instructions. Treatments were administered 24 h after transfection. The sequences of the RIG-I siRNA were: #1, 5′-CCCAACCGAUAUCAUUUCUdTdT-3′ and #2, 5′-CAGCUGACGUAAGAGUGAUdTdT-3′. The sequence of the scrambled control was: 5′-UUCUCCGAACGUGUCAC-GUdTdT-3′.

Plasmids construction. The wild-type expressing plasmid of human DDX58 (NM_014314) and mutant plasmid were constructed (Genomeditech, Shanghai, China). The RIG-I siRNA#2 combining sequence (5′-CAGCTGACGTAAGAGTGAT-3′) in wild-type RIG-I was under synonymous mutant (5′-cACCGCG-GATGTCAGGGTTat-3′) to generate mutant RIG-I. Both wild-type RIG-I and mutant RIG-I can encode the same RIG-I protein, however, siRNA#2 cannot combine with the RIG-I mRNA to degrade the RIG-I mRNA.

3-(4,5-Dimethylthiazol-2-yl)-2,5-diphenyltetrazolium bromide (MTT) assays. HN4 and HN30 cells were seeded in 96-well plates at a density of 3×10^3 cells per well. Human IFNα (PeproTech, Rocky Hill, NJ, USA), erlotinib (Selleck, Houston, TX, USA), nimotuzumab (Biotech Pharma, Beijing, China) and fludarabine (Selleck) were administrated at the indicated concentrations after cells had adhered. After a 72 h incubation, 20 μl of MTT were added to every well and incubated for 4 h. Then, 200 μl of DMSO were added to dissolve the formazan crystals in each well. The optical density (OD) was measured at 490 nm within 10 min.

Drug combination studies. In vitro drug combination studies were based on dose–effect curves generated by plotting the number of surviving cells in the MTT assay versus the dose after 72 h of treatment. For each cell line, the molar ratio of equipotent doses of the two agents (at the ratio of their IC50 values) was applied. The combination index (CI) was used to analyse the synergistic inhibitory effects of drug combinations using CompuSyn software according to the previously published Chou–Talalay equation (Chou, 2006). The general Equation for CI is given by

$$(D)1/(D_x)1 + (D)2/(D_x)2 == CI$$

In the denominators, $(D_x)1$ is the dose of drug 1 alone that inhibits x%. Likewise, $(D_x)2$ is the dose of drug 2 alone that inhibits x%. In the numerators, $(D)1$ is the proportion of drug 1 in the combination $(D)1 + (D)2$ that also inhibits x%. Likewise, $(D)2$ is the proportion of drug 2 in the combination $(D)1 + (D)2$ that also inhibits x%. Thus, $(D)1 + (D)2$ also inhibit x%. CI < 1, CI = 1, and CI > 1 indicate synergism, an additive effect, and antagonism, respectively; r represents the correlation coefficient determined from the median-effect plot (a value > 0.95 indicates goodness of fit). Fa represents the fraction of the population affected by the specified dose of the treatment. In our study, the Fa–CI plot

showed both actual data points and a simulated curve with a constant ratio.

The dose-reduction index (DRI) represents the order of magnitude (fold) of dose reduction obtained for the ED50 effect in a combination treatment compared with each drug alone. From the series of equations, the DRI value for the $x\%$ inhibition is calculated as: $(D_x)n/(D)n = (DRI)n$.

Flow cytometry. Flow cytometry was performed using a previously described method (Fang *et al.*, 2016). In brief, HN4 and HN30 cells were incubated with the indicated treatment for 48 h. Cells were suspended in 400 μl 1 × binding buffer, then added 5 μl Annexin V-FITC (BD Biosciences, Franklin Lake, NJ, USA) to the cell suspension, and incubated on ice for 30 mins. Then 5 μl propidium iodide (PI) was added and incubated on ice for 5 mis. All the procedure should protect from prolonged exposure to light. After PBS wash, cells were resuspended in 100 μl of binding buffer and analysed on a BD FORTASA flow cytometer. The final results were analysed with FlowJo software. For the cell cycle analysis, cells that had been exposed to the indicated treatment were fixed with 70% ethanol overnight. Cells were then washed and incubated with a PI/RNase staining kit (BD). For the Dc and natural killer cell analysis, peripheral blood monocytes (PBMC) were extracted from nude mice and analysed with the following antibodies and Fixable Viability Dye (eBioscience, San Diego, CA, USA), a FITC-I-A/I-E antibody, APC-CD11c antibody, and PE-CD49b antibody (all purchased from BD Biosciences). The subsequent steps performed as described above.

Immunoprecipitation and western blot assay. Western blot assays were performed using previously described methods (Jin *et al.*, 2015). The antibodies used in this study were: Stat1, p-Stat1 (Tyr701), Akt, p-Akt (Ser473), ERK1/2, p-ERK1/2 (Thr202/Tyr204), PARP, cleaved PARP, p-Rb (Ser807/811), p53, cyclin D1, ubiquitin, and cleaved caspases 1, 3, 8, and 9 from Cell Signaling Technology (CST, Danvers, MA, USA). The RIG-I antibody was purchased from Abcam (Cambridge, MA, USA). GAPDH, α-tubulin, and β-actin antibodies (all purchased from Proteintech, Rocky Hill, NJ, USA) were used as an internal control. Immunoreactive bands were scanned and analysed using an Odyssey Infrared Imaging System (LI-COR Biosciences, Lincoln, NE, USA).

In vivo study. SPF BALB/c nude mice (nu/nu, aged 4 weeks, and weighing ∼20 g) were purchased from the Shanghai Laboratory Animal Center (Shanghai, China) and were housed in SPF facilities at Shanghai Ninth People's Hospital, Shanghai Jiao Tong University School of Medicine. The Laboratory Animal Care and Use Committees of the hospital approved all experimental procedures. The nude mouse tumour xenograft model was established with Cal27 cells, an HNSCC cell line exhibiting strong tumourigenicity *in vivo*. In brief, 1×10^6 cells were subcutaneously injected into the right flank of the nude mice. After the xenograft reached a mean diameter of 5 mm, the animals received various treatment regimes: (a) control (0.9% saline, i.p.); (b) IFNα (20 000 IU per day, s.c.); (c) erlotinib (50 mg kg^{-1} per day, i.g.); (d) nimotuzumab (10 mg kg^{-1} per day, i.p.); (e) IFNα + erlotinib; and (f) IFNα + nimotuzumab. Tumour sizes and animal weights were monitored every 3 days. Tumour volumes were calculated using the formula: (length × width^2/2). Mice were killed and tumour tissues were excised after 4 weeks. Peripheral blood was collected from nude mice in the control and IFNα groups. DCs and NK cells were analysed using PBMCs. Portions of tumour tissues and organs were fixed and embedded in the paraffin. Tissue sections (4 μm) were stained with haematoxylin and eosin. The terminal deoxynucleotidyl transferase dUTP nick end labelling (TUNEL) assay was used to detect apoptotic cells. A lentivirus vector containing human the *DDX58* gene and a recombinant

lentivirus harbouring siRNA#2 targeting *DDX58* were constructed and confirmed (Genomeditech). The Cal27 cell line was transfected with lentiviral vectors and treated with puromycin for 1 week to induce stable expression. Cells (1×10^6) stably transfected with the lentivirus were inoculated into the right flank of nude mice. Tumour sizes and animal weights were monitored weekly. Mice were killed and tumour tissues were excised after 5 weeks. The tumour tissues were preserved and detected by immunohistochemistry and PCR. This study was approved by Ethics Committee of Ninth People's Hospital, Shanghai Jiao Tong University School of Medicine (Shanghai, China).

Immunohistochemistry. Immunohistochemistry was operated according our previous study (Ma *et al.*, 2017b). In brief, the sections were heated by water bath at 100 with EDTA buffer (PH 10.0) for 20 min to retrieve antigen. The primary antibodies were rabbit monoclonal anti- RIG-I antibody (Abcam) and rabbit monoclonal anti-MX1 antibody (Proteintech). Immunohistochemistry and image analysis were performed to measure and analyse the mean optical density for MX1 and RIG-I in the animal experiments.

Real-time PCR. Real-time PCR was operated according to the manufacturer's instructions as previous described. The sequence of primers were as follows: human IFNA1, 5′-CCTGATGAATGCG-GACTCCA-3′ (forward), 5′-TAGCAGGGGTGAGAGTCTTTG-3′ (reverse) and GAPDH: 5′-CCTCTGACTTCAACAGCGAC-3′ (forward) and 5′-TCCTCTTGTGCTCTTGCTGG-3′ (reverse).

Chromatin immunoprecipitation. Chromatin immunoprecipitation (ChIP) was strictly performed according the protocol of the SimpleChIP Enzymatic Chromatin IP kit (CST) and our previous study (Ma *et al.*, 2017a). In brief, after treatment with 100 ng ml^{-1} IFNα for 48 h, HN4 and HN30 cells were fixed with 1% formaldehyde for 10 min. Five microliters of the p-Stat1 (Tyr701) antibody or normal rabbit IgG were added to the corresponding samples. 30 μl of ChIP-grade Protein G Magnetic beads were added to the mixture and incubated for 2 h at 4 °C with rotation. A quantitative polymerase chain reaction analysis of the purified ChIP DNA (ChIP-qPCR) was performed to calculate the percent enrichment of the promoter region using the $2^{-\Delta\Delta CT}$ formula. The primers for the *DDX58* promoter were: Forward: 5′-GATGTCACT TCTCCCCAAGTTT-3′ and Reverse: 5′-GAGACAAGGTCTCAC TCTGTCTCC-3′.

Luciferase reporter assay. Luciferase assays were used to confirm the transcriptional activation of *DDX58* by IFNα. Cells were seeded in 12-well plates (1×10^5 cells per well) and grown to 40–50% confluence. Each *DDX58* promoter-luciferase construct was co-transfected into cells with pRL-TK (TK promoter Renilla luciferase construct as internal control). HN4 and HN30 cells were transiently transfected using the Lipofectamine 3000 transfection reagent (Invitrogen). Then, the indicated concentrations of IFNα were added 24 h after transfection. Luciferase activity was determined 24 h after stimulation using a dual-luciferase reporter assay system (Beyotime, Shanghai, China). In brief, cell lysates (200 μl per well) were used to measure the relative luciferase units in a luminometer by first mixing the cell lysates (20 μl) with 100 μl of luciferase assay reagent to measure firefly luciferase activity and subsequently adding 100 μl of Renilla luciferase reagent to measure Renilla luciferase activity. Data were normalised to Renilla luciferase activity (internal control) and presented as arbitrary units. All experiments were performed in triplicate.

Data mining. We performed data mining using the publicly available TCGA database (http://www.cbioportal.org/) to explore the correlation between the signal transducers and activators of transcription 1 (STAT1) mRNA and DDX58 mRNA in HNSCC tissues. The STAT1 co-expression data were mined from 279

HNSCC samples in the TCGA database (Cerami et al., 2012; Gao et al., 2013). The transcription factor-binding sites in the human DDX58 gene were predicted using JASPAR (http://jaspar.gener-eg.net/) (Wasserman and Sandelin (2004)).

Statistics. Statistical analyses were performed with SPSS 13.0 software for Windows (SPSS Inc., Chicago, IL, USA). Excel and GraphPad Prism version 6 (GraphPad Software, San Diego, CA, USA) were employed to process the initial data and plot the results. The CI was calculated with CompuSyn software to analyse the synergistic inhibitory effect of the drug combinations. Student's t-test and one-way analysis of variance were performed to assess the statistical significance of differences. $P < 0.05$ was considered statistically significant. * $P < 0.05$ and ** $P < 0.01$. All values are expressed as means ± s.d.

RESULTS

IFNα enhances the antitumour effects of erlotinib and nimotuzumab on HNSCC cells. We first detected whether IFNα enhanced the antitumour effects of erlotinib and nimotuzumab on HNSCC cells. Certain concentrations of IFNα enhanced the tumour inhibitory effects of erlotinib and nimotuzumab on HN4 and HN30 cells (Figure 1A and B), and the cell viability of the combination group was significantly less than the groups treated with erlotinib or nimotuzumab alone (Figure 1C). Conversely, the apoptotic fraction was significantly increased in the combination group using flow cytometry (Figure 1D, Supplementary Figure 1). Consistent with these findings, the levels of the IFNα downstream effector p-Stat1 (Tyr701) were markedly increased in both HN4 and HN30 cells following exposure to the combination treatment for up to 72 h compared with erlotinib or nimotuzumab alone (Figure 1E), suggesting that IFNα enhanced the killing effects of erlotinib and nimotuzumab in a p-stat1-dependent manner. No significance differences in p-AKT and p-ERK levels were observed in response to the IFNα combination treatment. Furthermore, we observed that IFNα, erlotinib, and nimotuzumab promoted the arrest of G1 phase (Figure 1F). Mechanically, IFNα promoted the expression of p53 in HN4 and HN30 cells, whereas erlotinib decreased the expression of p-Rb. IFNα combination with erlotinib and nimotuzumab (lane 5 and 6) significantly inhibited the expression of cyclin D1 than drugs alone, leading to cell cycle arrest and apoptosis (Supplementary Figure 2). Based on these results, a combination treatment with IFNα, erlotinib, and nimotuzumab cooperatively promoted G1 arrest and induced apoptosis in HN4 and HN30 cells. Moreover, we observed that the cell viability was significantly inhibited in IFNα and cetuximab (another mAb of EGFR) combined group than each alone (Figure 1G). Furthermore, we constructed erlotinib-resistant and nimotuzumab-resistant cell lines (Supplementary Figure 3) and observed that lower dose of IFNα could notably enhance the effect of EGFR inhibitors in drug-resistant HNSCC cell lines (Figure 1H). These results confirmed that IFNα enhanced the antiproliferative effects of erlotinib/nimotuzumab in HNSCC cells.

IFNα exerts a synergistic antitumour effect with erlotinib and nimotuzumab on HNSCC cell lines. The combination index were calculated using the Chou–Talalay method to further explore the potential synergistic effects of IFNα and EGFR-targeted therapies on HNSCC cells. Serial dilutions of the three drugs were detected using equipotent doses of two agents (at the ratio of each IC50 value). Fa–CI curves showing the CI versus affected cells/cells killed by the drug combination are shown (Figure 2). The dimensionless value at Fa = 0.5 was calculated from Fa–CI curve. Although CI = 1 indicates additive effect in the absence of synergism or antagonism, CI < 1 indicates synergism, and CI = 1 indicates antagonism. From the Figure 2, all CI values at Fa = 0.5

were below the CI = 1 horizontal dotted line. The numerical values of CI were shown in Table 1 to confirm the synergistic effects of IFNα, erlotinib, and nimotuzumab in HNSCC cells. An IC50 (r) ⩾ 0.95 suggested a good fit of the curve. DRI was used to measure how many folds the dose of each drug in a synergistic combination may be reduced at a given effect level when compared with the doses of each drug alone. Thus, the IFNα, erlotinib, and nimotuzumab combination treatment exerted a synergistic effect on HNSCC.

Both IFNα- and EGFR-targeted therapies promote RIG-I expression in HNSCC cells. According to the results from our previous study, high levels of activated RIG-I induced by a virus infection significantly increase apoptosis and inhibit tumour growth in HNSCC. We speculated that RIG-I may be involved in the effects of the IFNα combination treatment. Based on bioinformatics and literature analyses, RIG-I was considered as one of the potential targets of both IFNα and EGF. Our results showed a positive correlation between STAT1 and the DDX58 mRNA that encoded the RIG-I protein in 207 patients with HNSCC (Figure 3A), and IFNα greatly induced the expression of the RIG-I protein in a dose- and time-dependent manner (Figure 3B). More importantly, caspases 1, 3, 8, and 9 were activated in response to the IFNα incubation, supporting the tumour inhibitory effect of IFNα. Furthermore, IFNα reversed the downregulation of RIG-I expression with a siRNA in HN4 and HN30 cells (Figure 3C). The siRNA targeting RIG-I decreased the apoptotic fraction compared with scramble with or without IFNα treatment in HN4 and HN30 cells, and decreased cleaved PARP expression under IFNα treatment. (Figure 3D, Supplementary Figure 4), indicating that RIG-I has a key role in IFNα-induced apoptosis. In contrast to IFNα, EGF induced a time-dependent inhibition of RIG-I (Figure 3E). MG132 could also reverse the degradation of RIG-I mediated by EGF (Figure 3F). We speculated that the inhibition of RIG-I expression by EGF depended on the activation of the ubiquitin degradation pathway. Consistent with this hypothesis, treatment with MG132 induced RIG-I ubiquitination in EGF-stimulated cells (Figure 3G). In further support of the inhibitory effect of EGF on RIG-I, the EGFR inhibitors erlotinib and nimotuzumab markedly promoted RIG-I expression with or without EGF stimulation in HN4 and HN30 cells (Figures 3H and I, Supplementary Figure 5). Based on these results, the combination of IFNα and EGFR-targeted therapies exerted a synergic effect on upregulating RIG-I expression in HNSCC.

IFNα enhances the effects of EGFR-targeted therapies in vivo. Next, we confirmed the in vitro results using human HNSCC xenografts in nude mice. First, the tumour volumes were significantly ($P < 0.05$) smaller in the combined drug group than in the groups treated with each individual agent (Figure 4A). Notably, although nimotuzumab exerted a moderate effect in vitro, it exhibited a remarkable tumour inhibitory effect in vivo. Similarly, the IFNα treatment noticeably ($P < 0.01$) inhibited tumour growth compared with the control. These results were also confirmed by measuring the weights of the resulting tumours (Figure 4B). In addition, according to the results of the TUNEL assay, IFNα increased the number of apoptotic cells in vivo when mice were also treated with erlotinib and nimotuzumab (Figure 4C). No significant toxic effects on important organs were observed in any treatment group (Figure 4D). Consistent with our in vitro observations (Figures 3B and C), RIG-I expression was dramatically induced in the IFNα-treated mice compared with the control (Figure 4E). PBMCs from nude mice were analysed by flow cytometry to determine whether IFNα stimulated the immune system. IFNα administration obviously increased the percentage of DCs (4.08 ± 0.46% vs 1.75 ± 0.61%, $P < 0.05$) (Supplementary Figure 6A). Moreover, the percentage of NK cells was also significantly elevated by the IFNα treatment (15.90 ± 2.78% vs
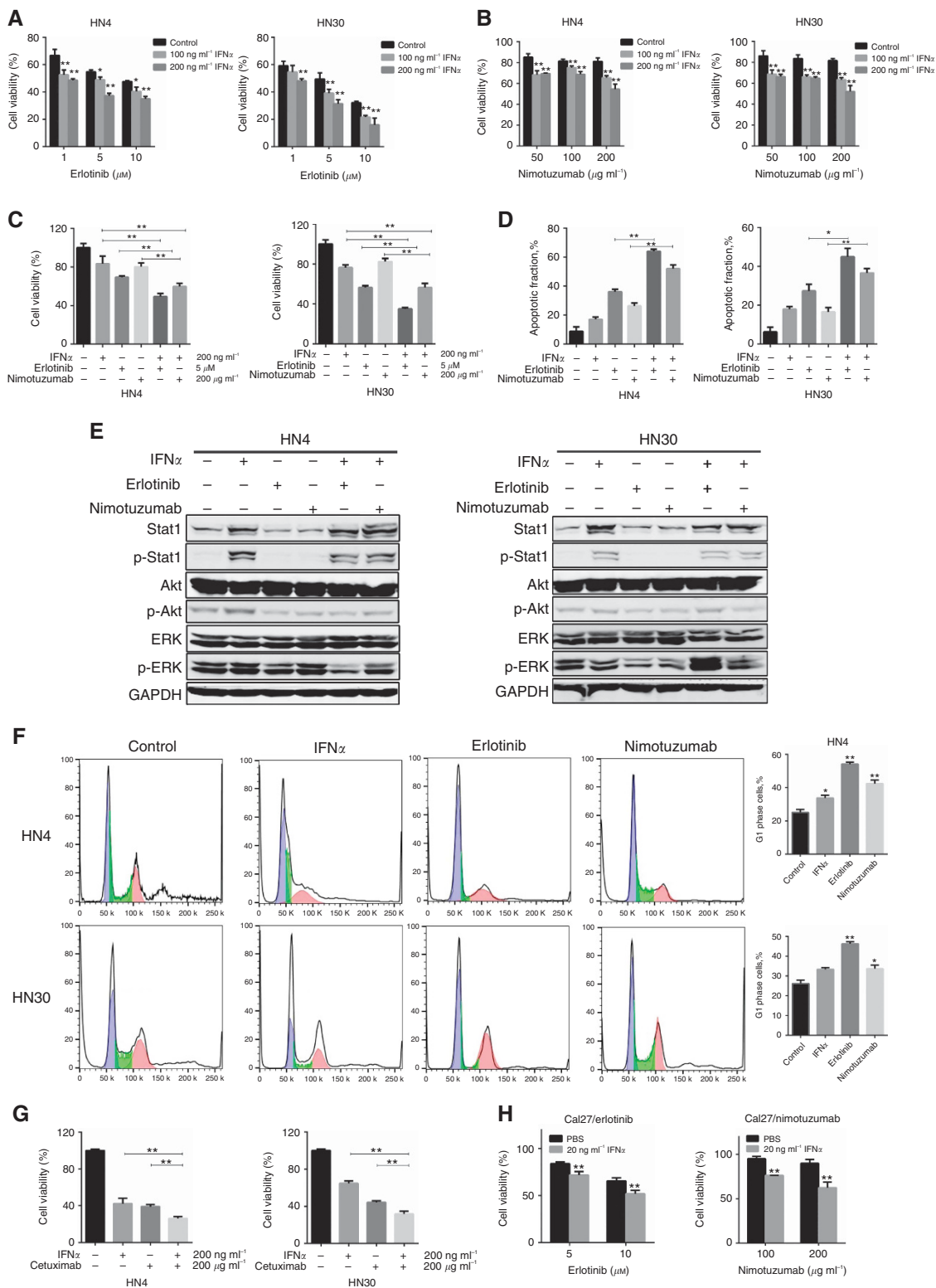
Figure 1. IFNα enhances the antitumour effects of erlotinib and nimotuzumab. (A) Cell viability was measured using the MTT assay after treatment with the indicated concentrations of erlotinib and IFNα for 72 h. (B) Cell viability was measured using the MTT assay after treatment with the indicated concentrations of IFNα and nimotuzumab for 72 h. (C) IFNα enhanced the antitumour effects of 72 h erlotinib and nimotuzumab treatments on HN4 and HN30 cells grown in a 96-well plate (3000 cells per well), as measured using the MTT assay. (D) IFNα increased the fraction of apoptotic HN4 and HN30 cells after treatment with erlotinib and nimotuzumab 72 h, as measured by a flow cytometry analysis of Annexin V and PI staining. (E) Cells were treated with IFNα (200 ng ml^{-1}), erlotinib (5 μM), and nimotuzumab (200 μg ml^{-1}) for 72 h. The possible downstream signals were analysed by western blotting. (F) The cell cycle was analysed using a flow cytometry analysis of PI staining after a 48 h treatment with IFNα (200 ng ml^{-1}), erlotinib (5 μM), and nimotuzumab (200 μg ml^{-1}). (G) The cell viability was measured by MTT under IFNα (200 ng ml^{-1}) and/or cetuximab (200 μg ml^{-1}) treatment for 72 h in HN4 and HN30. (H) Cell viability was measured after treatment with the indicated concentrations of erlotinib, nimotuzumab, and IFNα for 72 h in Cal27/erlotinib and Cal27/nimotuzumab cells. *$P < 0.05$, **$P < 0.01$.
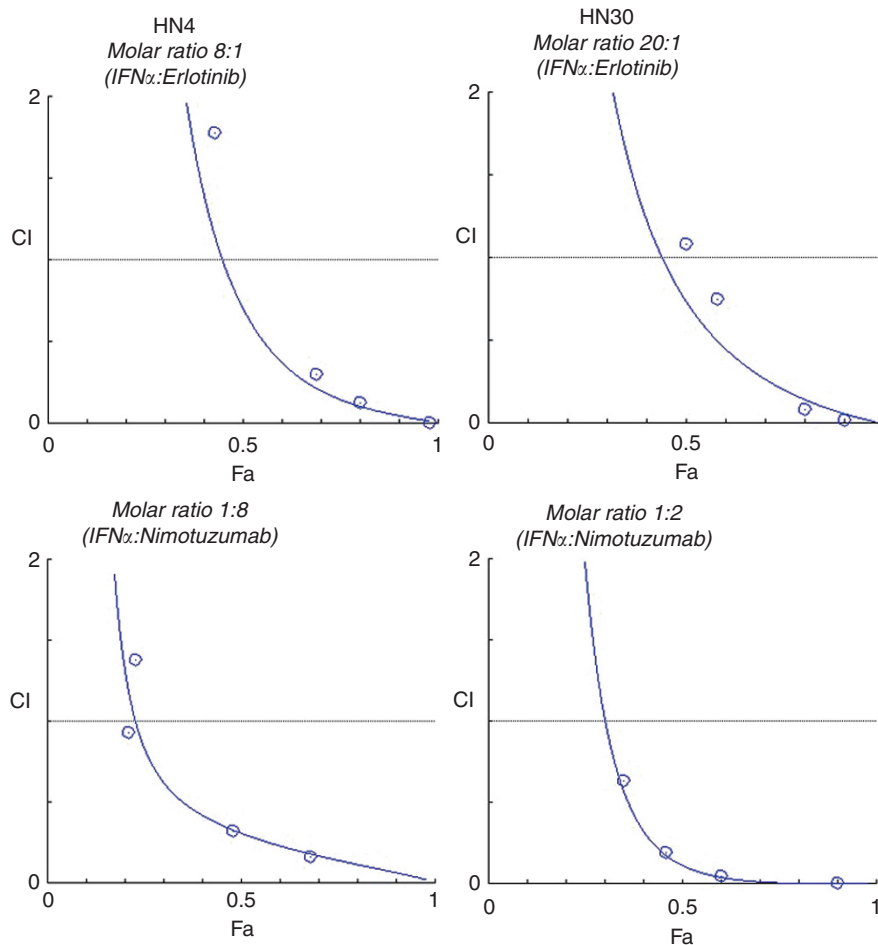
Figure 2. Synergistic antitumour effects of IFNα and EGFR-targeted therapies *in vitro*. Effects of treatments with combination of IFNα + erlotinib or nimotuzumab on HN4 and HN30 cell lines. The CI/fractional effect curve (Fa) showed the CI versus the fraction of cells affected/inhibited by the combination treatment in different cell lines. For each cell line, the molar ratio of equipotent doses of the two agents (at the ratio of their IC50$_S$) is shown. The combination analysis was performed using CompuSyn software.

Table 1. IC50 (r), DRI, and CI for IFNα combination treatment

| Cell lines | IC50 (r) | DRI at IC50 | | | CI |
		IFNα	Erlotinib	Nimotuzumab	
HN4	0.95247	10.3011	3.70441	–	0.36703
	0.98092	3.26596	–	371.503	0.30888
HN30	0.97663	7.70632	1.40254	–	0.84275
	0.97936	9.38196	–	298.758	0.10993

Abbreviations: CI = combination index; DRI = dose-reduction index; IFNα = interferon-alpha. IC50(r) represents the correlation coefficient for the fit between the CI and Fa. CIs were calculated for ED50 using an isobologram analysis generated with CompuSyn software. The DRI represents the order of magnitude (fold) of dose reduction obtained for the ED50 effect of the combination treatment compared with each drug alone.

$5.02 \pm 1.43\%$, $P < 0.01$, Supplementary Figure 6B). Overall, IFNα enhanced the antitumour effects of erlotinib and nimotuzumab and promoted RIG-I expression *in vivo*.

RIG-I overexpression inhibits tumour growth *in vivo*. A lentivirus vector expressing RIG-I was constructed and transfected into HNSCC cell lines to obtain stable cell lines and to test the function of RIG-I (Figure 5A). The xenograft tumours were smaller in mice in the RIG-I overexpression group than in the vector control group (Figure 5B). The tumour volumes and weights were

measured and the results showed that RIG-I overexpression markedly ($P < 0.01$) inhibited tumour growth compared with the vector, whereas RIG-I knockdown significantly ($P < 0.05$) promoted tumour growth (Figures 5C and D). Thus, in addition to acting as a well-known RLR against viral infection, RIG-I also functions as a tumour suppressor in HNSCC cells. Moreover, we detected whether RIG-I could induce immune response *in vivo*. MX1 is considered an ideal and specific marker for the activity of the IFNα signalling pathway (Silginer *et al.*, 2017). We observed that both RIG-I and MX1 were significantly increased in LV-RIG-I group than vector using immunohistochemistry (Figure 5E). Moreover, IFNA1 mRNA, encoding IFNα protein, also increased in LV-RIG-I group than vector (Figure 5F).

RIG-I knockdown reduces the sensitivity of HN4 and HN30 cells to IFNα, erlotinib, and nimotuzumab. An MTT assay was performed using transfected cells to determine whether RIG-1 regulated the sensitivity of HN4 and HN30 cells to IFNα, erlotinib, and nimotuzumab. RIG-I knockdown significantly reduced the sensitivity of HN4 and HN30 cells to 10, 100, and 1000 ng ml^{-1} IFNα (Figure 6A). RIG-I silencing significantly reduced the sensitivity of HN4 cells to 0.1, 1, 10, and 100 μM erlotinib and HN30 cells to 1, 10, and 100 μM erlotinib (Figure 6B). However, a significant difference in the sensitivity of HN4 cells to nimotuzumab was not observed. The viability of nimotuzumab-treated HN30 cells transfected with the RIG-I siRNA was significantly higher than of treated cells transfected with the scrambled siRNA
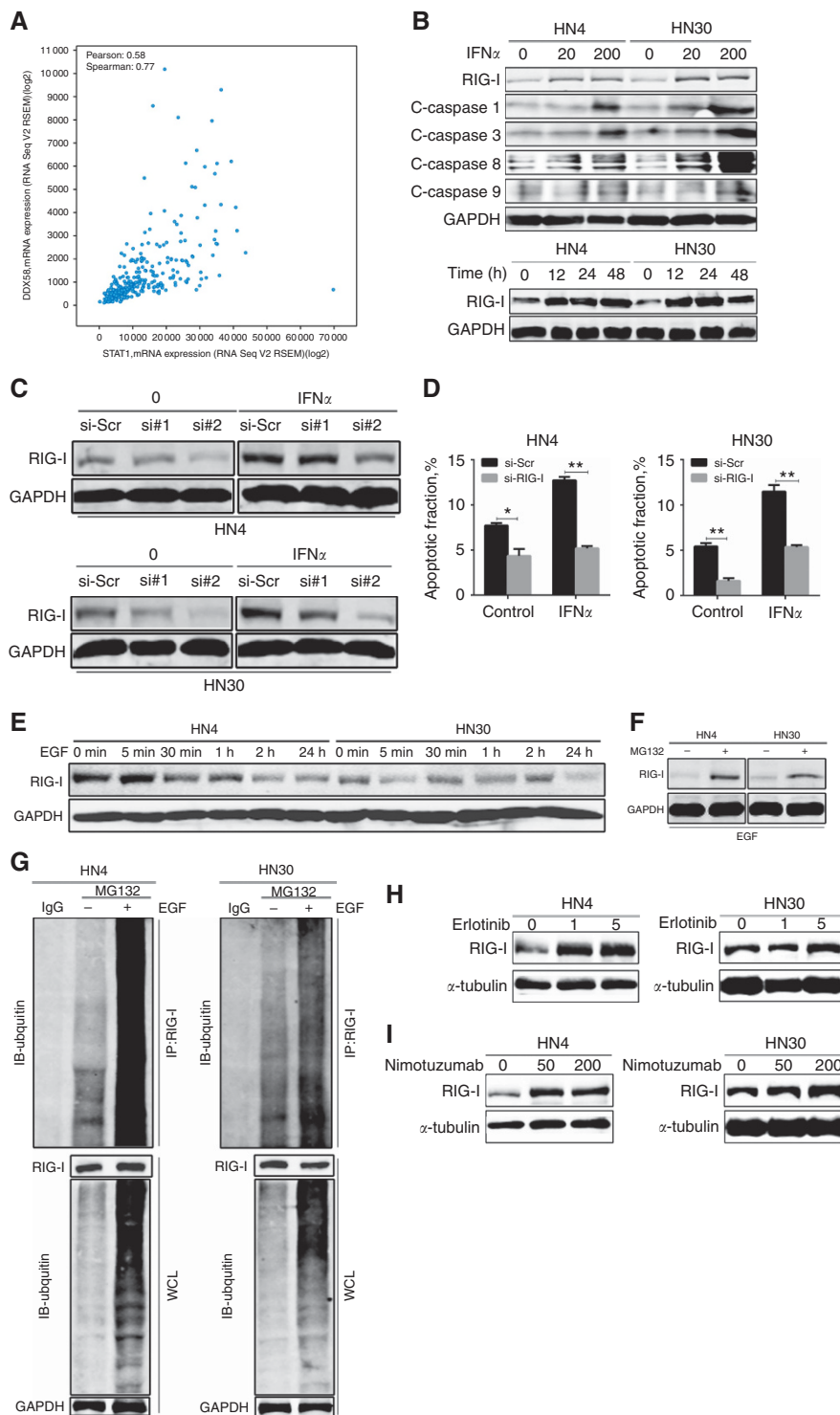
Figure 3. IFNα and EGFR-targeted therapies promote RIG-I expression in HN4 and HN30 cells. (A) The positive correlation observed between STAT1 and DDX58 mRNA in HNSCC was analysed using the TCGA database (Pearson's correlation coefficient: 0.58, Spearman's correlation coefficient: 0.77). (B) RIG-I expression was significantly induced after 48 h treatments with 20 or 200 ng ml^{-1} IFNα; caspases 1, 3, 8, and 9 were also activated. RIG-I expression was detected at the indicated times after treatment with 200 ng ml^{-1} IFNα. (C) HN4 and HN30 cells were transfected with siRNAs targeting RIG-I (#1 and #2) for 24 h and then treated with 100 ng ml^{-1} IFNα. RIG-I expression was detected by western blotting after 48 h. (D) After transfection with RIG-I siRNA#2 for 24 h, HN4, and HN30 cells were treated with PBS or 200 ng ml^{-1} IFNα for 48 h. The apoptosis cells were measured by flow cytometry analysis of Annexin V and PI staining. (E) HN4 and HN30 cells were starved overnight and then incubated with 50 ng ml^{-1} EGF for the indicated times to detect RIG-I degradation. (F) After serum starvation overnight, RIG-I was detected with or without 0.5 μM MG132 under 50 ng ml^{-1} EGF for 24 h in HN4 and HN30. (G) Cells were treated with or without 50 ng ml^{-1} EGF in medium containing 0.5 μM MG132 for 24 h. Immunoprecipitations were performed to examine the ubiquitination-mediated degradation of RIG-I in response to EGF stimulation. WCL: whole cell lysates. (H) Cells were treated with erlotinib (0, 1, or 5 μM) for 48 h to examine RIG-I expression. (I) RIG-I expression was detected after a 48 h treatment with nimotuzumab (0, 50, or 200 μg ml^{-1}). *$P < 0.05$, **$P < 0.01$.
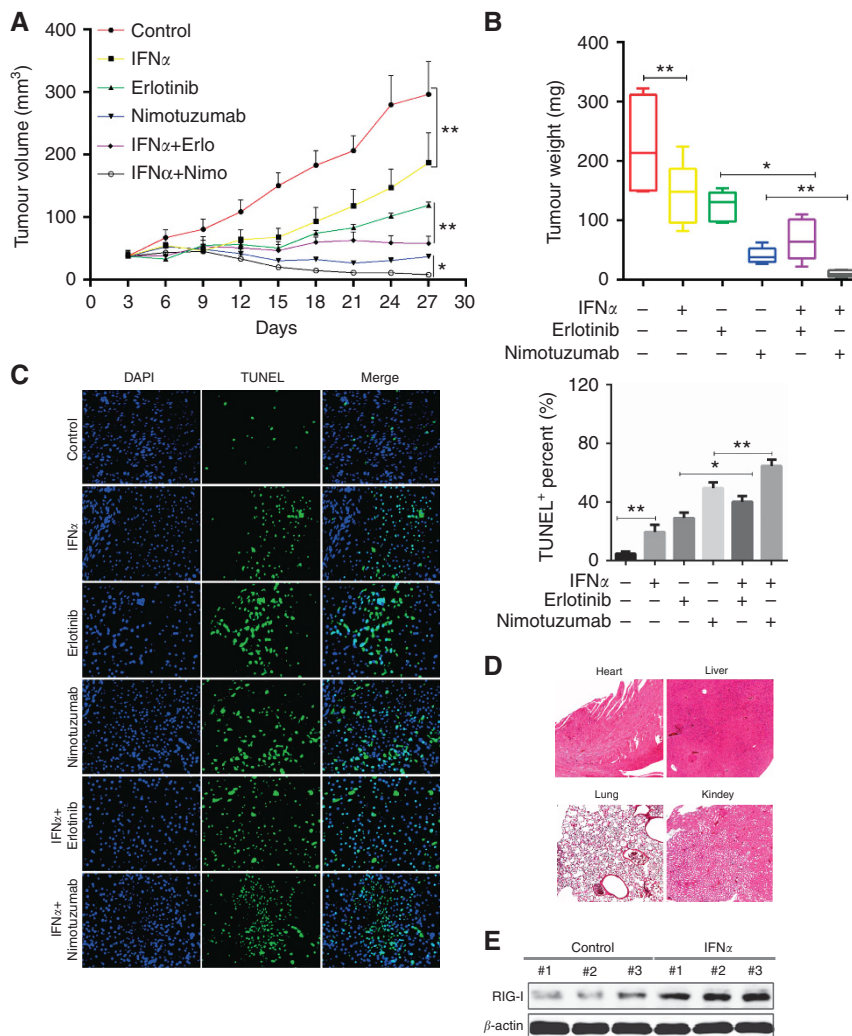
Figure 4. FNα enhances the antitumour activity of erlotinib and nimotuzumab *in vivo*. (**A**) After establishing the HNSCC tumour xenograft model, 30 nude mice were randomly divided into six groups (five mice per group). The groups received the following treatments: IFNα (20 000 IU per mouse per day, s.c.), erlotinib (50 mg kg^{-1} per day, i.g), nimotuzumab (10 mg kg^{-1} per day, i.p), IFNα plus erlotinib, IFNα plus nimotuzumab, and the control (0.9% saline, i.p). All mice were killed 27 days after treatment. The tumour volumes were analysed and compared among the groups. (**B**) Tumour weights were also measured and compared among the six groups. (**C**) The percentage of TUNEL-positive cells was counted in formalin-fixed paraffin embedding sections of tumours from each group. (**D**) Major organs from all mice were stained with haematoxylin and eosin to evaluate the safety of the combination treatment. (**E**) RIG-I expression was detected in western blots of freshly collected tumour tissues (3/5) from the control and IFNα groups. *$P < 0.05$, **$P < 0.01$.

(Figure 6C). After RIG-I knockdown, cells were more resistant to IFNα and EGFR inhibitors combination treatment (Figures 6D and E). RIG-I expression was not reduced by siRNA after synonymous mutant RIG-I plasmids transfection (Supplementary Figure 7A). Cell viability was significantly higher after co-transfection with siRNA for RIG-I and WT RIG-I plasmids than MT plasmids under IFNα and EGFR inhibitors combination treatment (Supplementary Figure 7B). Based on these *in vitro* results, the RIG-I expression level alters the sensitivity of HNSCC cells to IFNα, erlotinib, and nimotuzumab, and its expression may predict the response of HNSCC to IFNα and EGFR-targeted therapies.

IFNα transcriptionally regulates RIG-I expression through STAT1. Based on the results presented above, IFNα enhanced the inhibitory effects of erlotinib and nimotuzumab *in vitro* and *in vivo* by upregulating RIG-I expression in HNSCC. As shown in Figure 1, the effect of the combination of IFNα and EGFR-targeted therapies may depend on STAT1 activation. Therefore, we speculated that IFNα mainly upregulated RIG-I expression through STAT1 activation. Fludarabine specifically inhibits

STAT1 activation without affecting the phosphorylation of other STAT proteins (Meng *et al.*, 2007). The IC50 values of fludarabine for HN4 and HN30 cells were 0.9214 to 5.395 and 2.006 to 18.51 μM, respectively (Supplementary Figure 8). Fludarabine attenuated IFNα-induced RIG-I expression in both HN4 and HN30 cells (Figure 7A), supporting the hypothesis that STAT1 activation plays a major role in IFNα-induced RIG-I expression. STAT1 is one of the key downstream signal transducers and activators of IFNα, and IFNα-induced STAT1 phosphorylation at Tyr701 leads to STAT1 dimerisation, nuclear translocation, DNA binding, and the subsequent transcription of a series of immune-related target genes (Li *et al.*, 2014a). A publicly available schematic diagram of the binding motif of human STAT1 was shown in Supplementary Figure 9. Five putative STAT1 binding sites in *DDX58* promoter region were predicted by the JASPAR database (Supplementary Figure 10). Consistent with this prediction, p-Stat1 (Tyr701) bound the promoter region of the *DDX58* gene in IFNα-stimulated HN4 and HN30 cells in the ChIP assay (Figure 7B). A dual-luciferase reporter system was performed to test whether IFNα activated

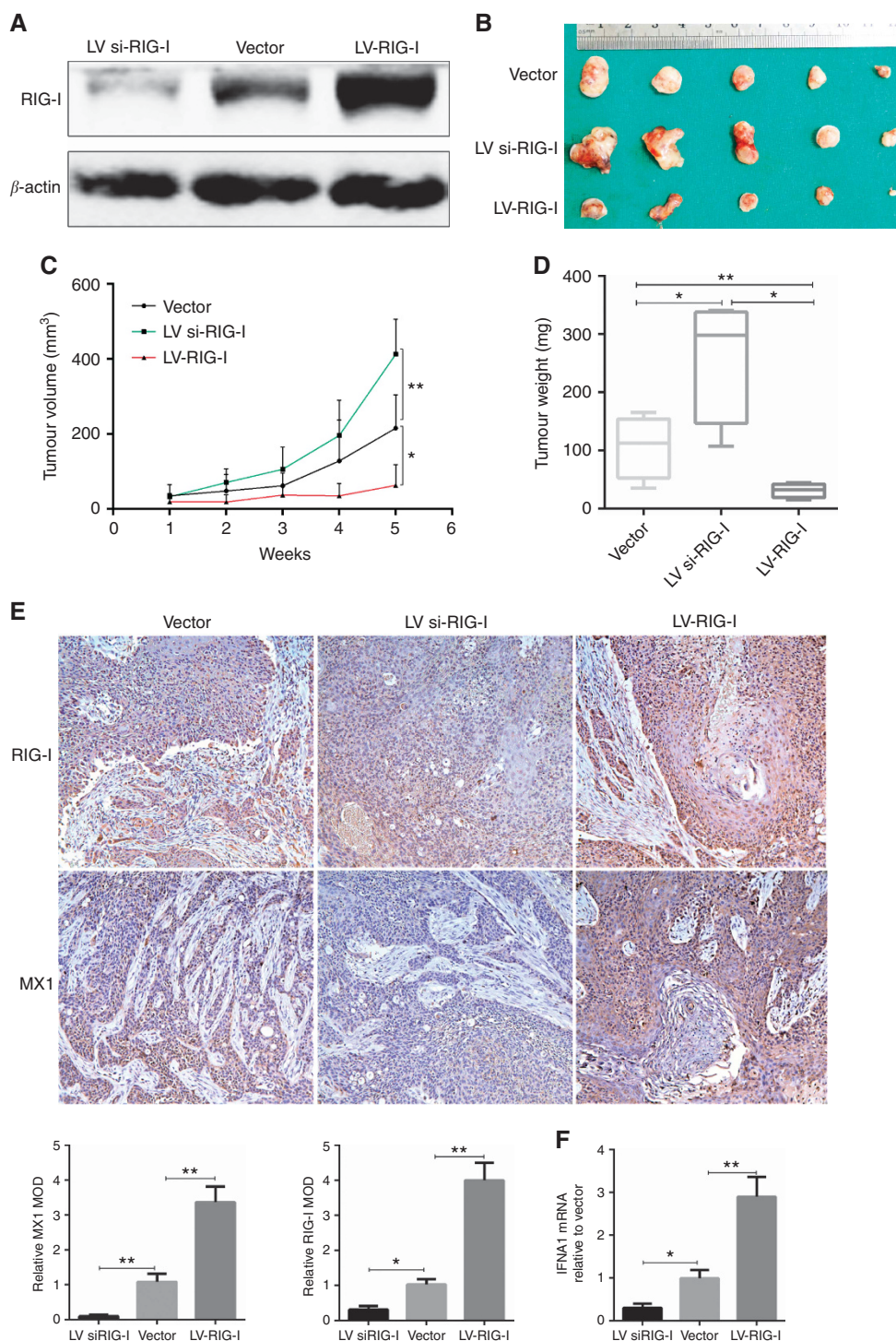**Figure 5. RIG-I overexpression inhibits tumour growth *in vivo*. (A)** The RIG-I expression level was detected in cell lines stably transfected with the lentivirus. **(B)** Tumours were collected from mice in the vector, LV si-RIG-I, and LV-RIG-I groups after killing (1×10^6 cells per mice, five mice per group). The lentivirus vector was used as control. **(C)** Tumour volumes were measured for 5 weeks and compared among three groups. **(D)** Tumour weights were measured in each group and compared. **(E)** Both RIG-I and MX1, a surrogate marker of IFNα activation, were detected and analysed using immunohistochemistry in the vector, LV si-RIG-I, and LV-RIG-I groups. **(F)** IFNA1 mRNA was measured using real-time PCR among three groups. magnification: $\times 200$. *$P < 0.05$, **$P < 0.01$.

DDX58 transcription. The activity of the *DDX58* promoter was significantly increased by IFNα stimulation in a dose-dependent manner (Figure 7C). In summary, IFNα transcriptionally activated RIG-I expression, whereas EGFR-targeted therapies blocked RIG-I degradation. Both IFNα and erlotinib/nimotuzumab synergistically promoted RIG-I expression to inhibit HNSCC tumour growth (Supplementary Figure 11).

DISCUSSION

Based on our comprehensive results, IFNα enhanced the antitumour activity of erlotinib and nimotuzumab in HNSCC by upregulating RIG-I expression both *in vitro* and *in vivo*. A clear synergistic antitumour effect of IFNα, erlotinib, and nimotuzumab
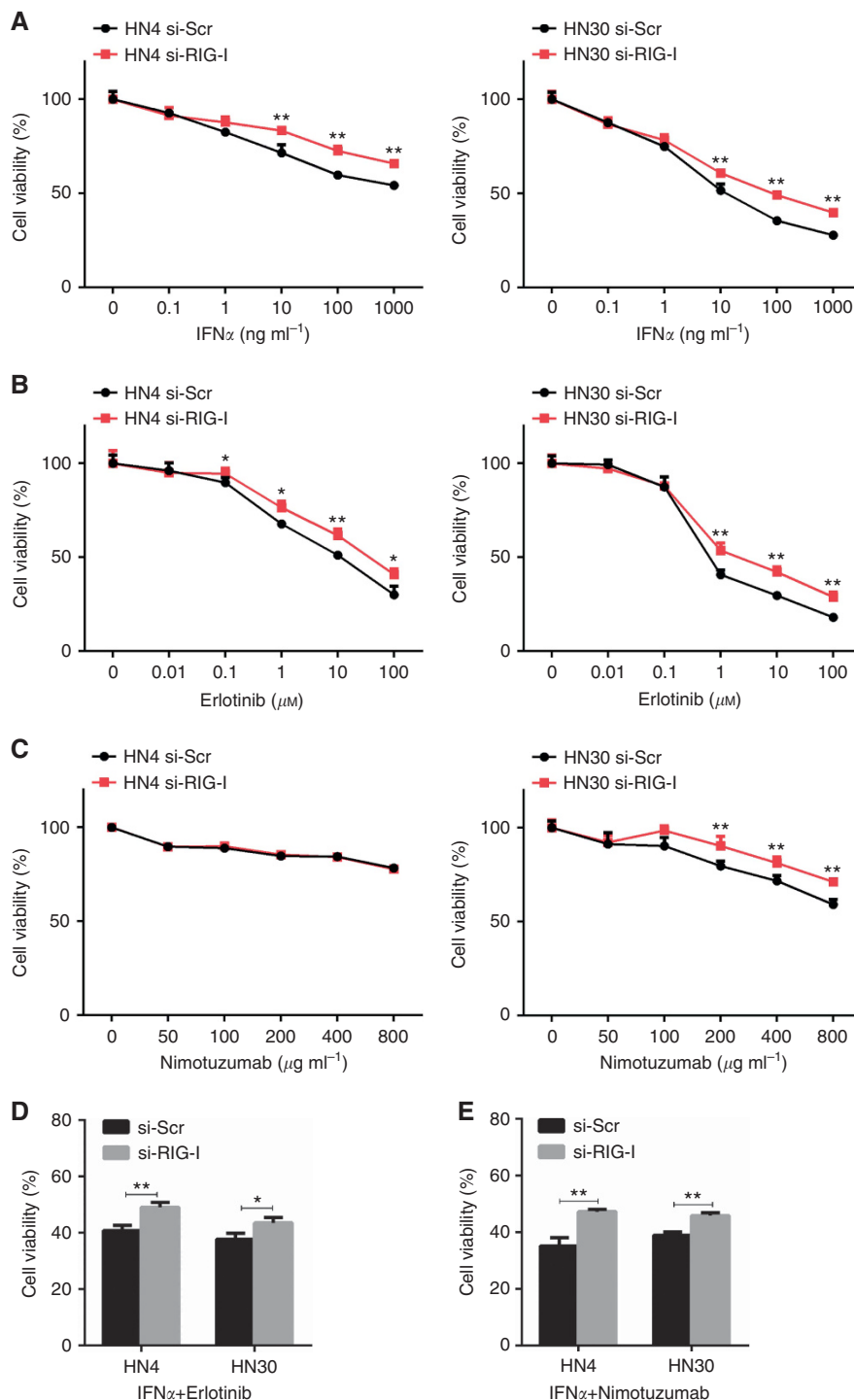
Figure 6. RIG-I knockdown reduces the sensitivity of HNSCC cells to IFNα, erlotinib, and nimotuzumab. (A) Twenty-four hours after transfection with siRNAs targeting RIG-I, cells were seeded in 96-well plate at a density of 3×10^3 cells per well. Cells were then incubated with the indicated concentrations of IFNα for 72 h. Cell viability was determined using the MTT assay. (B) Transfected cells were incubated with erlotinib for 72 h. Cell viability was measured and compared. (C) Twenty-four hours after transfection with siRNAs targeting RIGI-I, cells were treated with nimotuzumab for 72 h. (D) After siRNA transfection for 24 h, cells were incubated with 200 ng ml^{-1} IFNα and 5 μM erlotinib for 72 h. Cell viability was determined using the MTT assay. (E) After transfection for 24 h, cells were treated with 200 ng ml^{-1} IFNα and 200 μg ml^{-1} nimotuzumab for 72 h. *$P < 0.05$ and **$P < 0.01$.

was observed in the median drug analysis and CI calculation. This finding is of great significance to the clinical application of the combination treatment with IFNα and EGFR-targeted drugs to HNSCC.

IFNα is a cytokine with multiple functions that exerts a chemosensitising effect on several tumours. In colon and bladder cancer cell lines, IFNα only promotes the antiproliferative effect of erlotinib in assays using crystal-violet staining (Yang et al., 2005, 2007). However, the two previous studies were operated by the same author who used a less-effective method of analysis, crystal-violet staining. A combination treatment including gefitinib and IFNα produces a synergistic antiproliferative effect in vitro and
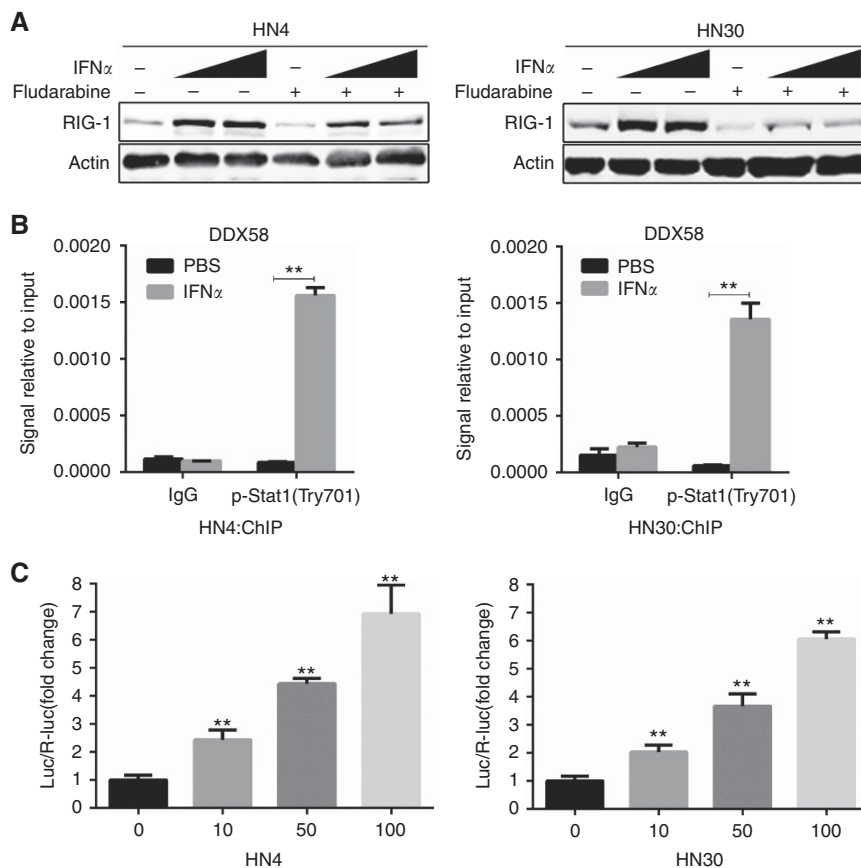
Figure 7. IFNα activates RIG-I transcription in HNSCC cells through p-STAT1 (Tyr701). (**A**) HN4 and HN30 cells were treated with IFNα (0, 20, or 200 ng ml^{-1}) and fludarabine (0.5 μM) for 48 h, and RIG-I expression was detected. Beta-actin was used as an internal control. (**B**) HN4 and HN30 cells were incubated with 100 ng ml^{-1} IFNα for 48 h. The ChIP assay was performed with p-Stat 1 (Tyr701) and normal rabbit IgG antibodies. Enrichment of *DDX58* promoter regions was calculated using real-time PCR (Percent input = 2% × 2$^{(C[T]\ 2\%Input\ Sample\ -\ C[T]\ IP\ Sample)}$). (**C**) *DDX58* promoter activity was detected in HN4 and HN30 cells 24 h after stimulation with IFNα. ChIP = chromatin immunoprecipitation. **$P < 0.01$.

induces a delay in tumour growth and increases the survival rate of nude mice with established HNSCC xenografts (Bruzzese *et al.*, 2006). However, few studies have examined the effects of a combination treatment comprising IFNα and EGFR mAbs, which may utilise a different mechanism to inhibit EGFR signalling. Several *in vitro* and *in vivo* experiments were applied in this study to confirm the synergistic effects of IFNα and erlotinib/nimotuzumab on HNSCC. To our surprise, human IFNα increased the percentages of NK cells and DCs in nude mice to trigger the mouse immune system, but the underlying mechanism remains unclear. Nimotuzumab represents the first human mAb against EGFR to be approved as a treatment for HNSCC. In our study, nimotuzumab moderately inhibited tumour cell growth *in vitro*, whereas it exerted a strong inhibitory effect *in vivo*. This phenomenon is interesting and reminds us of the difference between *in vitro* and *in vivo* environments. Our study was the first to simultaneously investigate both TKIs and mAbs of EGFR in combination with IFNα as a treatment for HNSCC. These results will be very significant for clinical applications of the combination of IFNα with erlotinib and nimotuzumab in the future.

The synergistic effect of IFNα and erlotinib/nimotuzumab mainly depended on RIG-I activation, which directly inhibited tumour growth. This novel mechanism for the combination of IFNα and EGFR-targeted therapies in HNSCC improves our understanding of the effects of the IFNα combination treatment. The upregulation of EGFR expression in response to an IFNα treatment is considered an escape mechanism from resistance to EGFR-targeted therapies (Budillon *et al.*, 1991; Caraglia *et al.*, 1995). These previous observations were partially attributed to an

EGF-dependent survival pathway and IFNα-induced ERK activation. RIG-I is one of the most important RLRs for detecting viral RNA and initiating the innate immune response. Based on our results, innate immunity might have an important role in the effects of EGFR-targeted therapies.

In our study, a novel tumour suppressor function of RIG-I was confirmed in HNSCC. In a cohort of patients with HBV-associated hepatocellular carcinoma, high intratumour levels of the cytosolic RIG-I protein predicted the response to IFNα therapy, and the depletion of RIG-I from HCC xenografts compromised the antineoplastic effects of IFNα on mice (Hou *et al.*, 2014). RIG-I silencing reduced the sensitivity of HNSCC cells to IFNα, erlotinib, and nimotuzumab in our study. Therefore, the upregulation of RIG-I expression plays an important role in modulating the effects of IFNα and EGFR-targeted therapies and inhibiting tumour growth in HNSCC. Thus, RIG-I is required for an effective response to IFNα in patients. Moreover, EGFR inhibitors blocked EGF-induced RIG-I ubiquitination to upregulate RIG expression in HNSCC cell lines. However, the mechanism by which EGF stimulation induces RIG-I ubiquitination in HNSCC requires further investigation. The activation of the RIG-I pathway by a virus infection promotes the transcription of IFNα and antiviral enzymes. RIG-I expression was significantly induced by IFNα in tumour cells in our study. The positive feedback loop between IFNα and RIG-I provided a new insight into the effects of the combination of IFNα and EGFR inhibitors. The therapeutic effects of IFNα and EGFR-targeted therapies greatly relied on RIG-I expression. Virus RNA-unprimed RIG-I alters its conformation and functional states to disrupt the association between Src and

AKT and inhibit tumour proliferation (Li *et al.*, 2014b). This finding may explain the tumour suppressor function of RIG-I in HNSCC. Patients with higher RIG-I expression in HNSCC tissues may benefit from IFNα and EGFR-targeted therapies. Assessments of the expression of RIG-I in biopsy tissues from patients with HNSCC could be applied to select patients who would benefit from the combination treatment. RIG-I may be a predictive marker for the use of a combination of IFNα and EGFR-targeted therapies in patients with HNSCC in future clinical investigations.

In conclusion, IFNα enhanced the antitumour effects of erlotinib and nimotuzumab by upregulating RIG-I expression, providing a strong rationale for tests of the therapeutic efficacy of EGFR-targeted therapies (erlotinib and nimotuzumab) in combination with IFNα as a treatment for HNSCC in future clinical trials. Moreover, RIG-I expression may be an effective predictor of the effectiveness of the IFNα combination treatment in patients with HNSCC.

ACKNOWLEDGEMENTS

CONFLICT OF INTEREST

The authors declare no conflict of interest.

REFERENCES

Agulnik M (2012) New approaches to EGFR inhibition for locally advanced or metastatic squamous cell carcinoma of the head and neck (SCCHN). *Med Oncol* **29**: 2481–2491.

Bacher N, Raker V, Hofmann C, Graulich E, Schwenk M, Baumgrass R, Bopp T, Zechner U, Merten L, Becker C, Steinbrink K (2013) Interferon-alpha suppresses cAMP to disarm human regulatory T cells. *Cancer Res* **73**: 5647–5656.

Braig F, Kriegs M, Voigtlaender M, Habel B, Grob T, Biskup K, Blanchard V, Sack M, Thalhammer A, Ben Batalla I, Braren I, Laban S, Danielczyk A, Goletz S, Jakubowicz E, Markl B, Trepel M, Knecht R, Riecken K, Fehse B, Loges S, Bokemeyer C, Binder M (2017) Cetuximab resistance in head and neck cancer is mediated by EGFR-K521 polymorphism. *Cancer Res* **77**: 1188–1199.

Bruzzese F, Di Gennaro E, Avallone A, Pepe S, Arra C, Caraglia M, Tagliaferri P, Budillon A (2006) Synergistic antitumor activity of epidermal growth factor receptor tyrosine kinase inhibitor gefitinib and IFN-alpha in head and neck cancer cells in vitro and in vivo. *Clin Cancer Res* **12**: 617–625.

Budillon A, Tagliaferri P, Caraglia M, Torrisi MR, Normanno N, Iacobelli S, Palmieri G, Stoppelli MP, Frati L, Bianco AR (1991) Upregulation of epidermal growth factor receptor induced by alpha-interferon in human epidermoid cancer cells. *Cancer Res* **51**: 1294–1299.

Caraglia M, Abbruzzese A, Leardi A, Pepe S, Budillon A, Baldassare G, Selleri C, Lorenzo SD, Fabbrocini A, Giuberti G, Vitale G, Lupoli G, Bianco AR, Tagliaferri P (1999) Interferon-alpha induces apoptosis in human KB cells through a stress-dependent mitogen activated protein kinase pathway that is antagonized by epidermal growth factor. *Cell Death Differ* **6**: 773–780.

Caraglia M, Leardi A, Corradino S, Ciardiello F, Budillon A, Guarrasi R, Bianco AR, Tagliaferri P (1995) alpha-Interferon potentiates epidermal growth factor receptor-mediated effects on human epidermoid carcinoma KB cells. *Int J Cancer* **61**: 342–347.

Cerami E, Gao J, Dogrusoz U, Gross BE, Sumer SO, Aksoy BA, Jacobsen A, Byrne CJ, Heuer ML, Larsson E, Antipin Y, Reva B, Goldberg AP,

Sander C, Schultz N (2012) The cBio cancer genomics portal: an open platform for exploring multidimensional cancer genomics data. *Cancer Discov* **2**: 401–404.

Chou TC (2006) Theoretical basis, experimental design, and computerized simulation of synergism and antagonism in drug combination studies. *Pharmacol Rev* **58**: 621–681.

Diaz A, Batista AE, Montero E (2009) Interferon-alpha conditioned sensitivity to an anti-epidermal growth factor receptor monoclonal antibody in a human lung cancer cell line with intermediate expression of the receptor. *J Interferon Cytokine Res* **29**: 433–440.

Fang S, Huang Y, Wang S, Zhang Y, Luo X, Liu L, Zhong S, Liu X, Li D, Liang R, Miranda P, Gu P, Zhou H, Fan X, Li B (2016) IL-17 A exacerbates fibrosis by promoting the proinflammatory and profibrotic function of orbital fibroblasts in TAO. *J Clin Endocrinol Metab* **101**: 2955–2965.

Gao J, Aksoy BA, Dogrusoz U, Dresdner G, Gross B, Sumer SO, Sun Y, Jacobsen A, Sinha R, Larsson E, Cerami E, Sander C, Schultz N (2013) Integrative analysis of complex cancer genomics and clinical profiles using the cBioPortal. *Sci Signal* **6**: pl1.

Hou J, Zhou Y, Zheng Y, Fan J, Zhou W, Ng IO, Sun H, Qin L, Qiu S, Lee JM, Lo CM, Man K, Yang Y, Yang Y, Yang Y, Zhang Q, Zhu X, Li N, Wang Z, Ding G, Zhuang SM, Zheng L, Luo X, Xie Y, Liang A, Wang Z, Zhang M, Xia Q, Liang T, Yu Y, Cao X (2014) Hepatic RIG-I predicts survival and interferon-alpha therapeutic response in hepatocellular carcinoma. *Cancer Cell* **25**: 49–63.

Hu J, He Y, Yan M, Zhu C, Ye W, Zhu H, Chen W, Zhang C, Zhang Z (2013) Dose dependent activation of retinoic acid-inducible gene-I promotes both proliferation and apoptosis signals in human head and neck squamous cell carcinoma. *PLoS One* **8**: e58273.

Imai K, Takaoka A (2006) Comparing antibody and small-molecule therapies for cancer. *Nat Rev Cancer* **6**: 714–727.

Jin SF, Ma HL, Liu ZL, Fu ST, Zhang CP, He Y (2015) XL413, a cell division cycle 7 kinase inhibitor enhanced the anti-fibrotic effect of pirfenidone on TGF-beta1-stimulated C3H10T1/2 cells via Smad2/4. *Exp Cell Res* **339**: 289–299.

Joffre OP, Segura E, Savina A, Amigorena S (2012) Cross-presentation by dendritic cells. *Nat Rev Immunol* **12**: 557–569.

Li W, Wei Q, Liang J (2014a) Phosphorylated signal transducer and activator of transcription 1 is a potential predictor of interferon response in patients with advanced renal cell carcinoma. *Mol Med Rep* **9**: 1929–1934.

Li XY, Jiang LJ, Chen L, Ding ML, Guo HZ, Zhang W, Zhang HX, Ma XD, Liu XZ, Xi XD, Chen SJ, Chen Z, Zhu J (2014b) RIG-I modulates Src-mediated AKT activation to restrain leukemic stemness. *Mol Cell* **53**: 407–419.

Ma H, Jin S, Yang W, Tian Z, Liu S, Wang Y, Zhou G, Zhao M, Gvetadze S, Zhang Z, Hu J (2017a) Interferon-alpha promotes the expression of cancer stem cell markers in oral squamous cell carcinoma. *J Cancer* **8**: 2384–2393.

Ma HL, Jin SF, Ju WT, Fu Y, Tu YY, Wang LZ, Jiang L, Zhang ZY, Zhong LP (2017b) Stathmin is overexpressed and regulated by mutant p53 in oral squamous cell carcinoma. *J Exp Clin Cancer Res* **36**: 109.

Martinez-Useros J and Garcia-Foncillas J (2015) The challenge of blocking a wider family members of EGFR against head and neck squamous cell carcinomas. *Oral Oncol* **51**: 423–430.

Meng H, Yang C, Ni W, Ding W, Yang X, Qian W (2007) Antitumor activity of fludarabine against human multiple myeloma in vitro and in vivo. *Eur J Haematol* **79**: 486–493.

Parker BS, Rautela J, Hertzog PJ (2016) Antitumour actions of interferons: implications for cancer therapy. *Nat Rev Cancer* **16**: 131–144.

Sacco AG, Cohen EE (2015) Current treatment options for recurrent or metastatic head and neck squamous cell carcinoma. *J Clin Oncol* **33**: 3305–3313.

Sharafinski ME, Ferris RL, Ferrone S, Grandis JR (2010) Epidermal growth factor receptor targeted therapy of squamous cell carcinoma of the head and neck. *Head Neck* **32**: 1412–1421.

Silginer M, Nagy S, Happold C, Schneider H, Weller M, Roth P (2017) Autocrine activation of the IFN signaling pathway may promote immune escape in glioblastoma. *Neuro Oncol* **19**(10): 1338–1349.

Srivastava S, Koch MA, Pepper M, Campbell DJ (2014) Type I interferons directly inhibit regulatory T cells to allow optimal antiviral T cell responses during acute LCMV infection. *J Exp Med* **211**: 961–974.

Vermorken JB, Mesia R, Rivera F, Remenar E, Kawecki A, Rottey S, Erfan J, Zabolotnyy D, Kienzer HR, Cupissol D, Peyrade F, Benasso M, Vynnychenko I, De Raucourt D, Bokemeyer C, Schueler A, Amellal N, Hitt R (2008) Platinum-based chemotherapy plus cetuximab in head and neck cancer. *N Engl J Med* **359**: 1116–1127.

Vermorken JB, Stohlmacher-Williams J, Davidenko I, Licitra L, Winquist E, Villanueva C, Foa P, Rottey S, Skladowski K, Tahara M, Pai VR, Faivre S, Blajman CR, Forastiere AA, Stein BN, Oliner KS, Pan Z, Bach BA (2013) Cisplatin and fluorouracil with or without panitumumab in patients with recurrent or metastatic squamous-cell carcinoma of the head and neck (SPECTRUM): an open-label phase 3 randomised trial. *Lancet Oncol* **14**: 697–710.

Wasserman WW and Sandelin A (2004) Applied bioinformatics for the identification of regulatory elements. *Nat Rev Genet* **5**: 276–287.

Weber-Gerlach M, Weber F (2016) Standing on three legs: antiviral activities of RIG-I against influenza viruses. *Curr Opin Immunol* **42**: 71–75.

Wen Y, Grandis JR (2015) Emerging drugs for head and neck cancer. *Expert Opin Emerg Drugs* **20**: 313–329.

Yang JL, Qu XJ, Hayes VM, Brenner PC, Russell PJ, Goldstein D (2007) Erlotinib (OSI-774)-induced inhibition of transitional cell carcinoma of bladder cell line growth is enhanced by interferon-alpha. *BJU Int* **99**: 1539–1545.

Yang JL, Qu XJ, Russell PJ, Goldstein D (2005) Interferon-alpha promotes the anti-proliferative effect of Erlotinib (OSI-774) on human colon cancer cell lines. *Cancer Lett* **225**: 61–74.

Supplementary Information accompanies this paper on British Journal of Cancer website (http://www.nature.com/bjc)